ChemPubSoc Europe

DOI: 10.1002/open.201900179

Open Access ChemistryOPEN Communications

Stabilization of Pancake Bonding in $(TCNQ)_2^{\bullet-}$ Dimers in the Radical-Anionic Salt (N–CH_3–2-NH_2–5Cl–Py)(TCNQ)(CH_3CN) Solvate and Antiferromagnetism Induction

Tetiana N. Starodub,[a] Erik Čižmár,[b] Andrii Kliuikov,[b] Vladimir A. Starodub,[a] Alexander Feher,[b] and Mariana Kozlowska*[c]

We report a new antiferromagnetic radical-anion salt (RAS) formed from 7,7,8,8-tetracyanquinonedimethane (TCNQ) anion and 2-amino-5-chloro-pyridine cation with the composition of (N–CH_3–2-NH_2–5Cl–Py)(TCNQ)(CH_3CN). The crystallographic data indicates the formation of $(TCNQ)_2^{\bullet-}$ radical-anion π-dimers in the synthesized RAS. Unrestricted density functional theory calculations show that the formed π-dimers characterize with strong π-stacking "pancake" interactions, resulting in high electronic coupling, enabling efficient charge transfer properties, but π-dimers cannot be stable in the isolated conditions as a result of strong Coulomb repulsions. In a crystal, where $(TCNQ)_2^{\bullet-}$ π-dimers bound in the endless chainlets via supramolecular bonds with (N–CH_3–2-NH_2–5-Cl–Py)$^+$ cations, the repulsion forces are screened, allowing for specific parallel π-stacking interactions and stable radical-anion dimers formation. Measurements of magnetic susceptibility and magnetization confirm antiferromagnetic properties of RAS, what is in line with the higher stability of ground singlet state of the radical-anion pair, calculated by means of the DFT. Therefore, the reported radical-anion (N–CH_3–2-NH_2–5Cl–Py)(TCNQ)(CH_3CN) solvate has promising applications in novel magnetics with supramolecular structures.

Radical-anion salts (RAS) based on 7,7,8,8-tetracyanquinonedimethane (TCNQ) have attracted researchers' interest since the 1960s.[1] The reason for this is their extraordinary electronic and magnetic properties, *i.e.* high anisotropic electrical conductivity, the ability to organize the magnetic structures for ferro- and antiferromagnetic behavior and manifestation of electron-phonon interactions in the oscillation spectra. Moreover, TCNQ radical anion has highly delocalized electronic structure, resulting in electronic transport and magnetically coupled interactions through π-π interactions along the stacking direction and formation of molecular solids with low-dimensional conducting and magnetic features.[2] As a result, TCNQ containing RAS are well-known compounds in micro- and nanoelectronics.[3]

In the series of our previous works,[4,5] we have shown the unique conductive properties of radical anion salts formed by TCNQ and $[M(N–N)_2]^{2+}$-cations (M=Mn, Fe, Co, Ni; N–N = phen, dipy) and formation of conductive materials as well as magnetically ordered structures. This includes ferro- and antiferromagnetic (AFM) materials and spin ladders. In the present communication, we report the formation of singlet-state $(TCNQ)_2^{\bullet-}$ radical-anion π-dimers in a new RAS TCNQ solvate, containing a cation based on 2-amino-5-chloro-pyridine (see Figure 1a).[6] This cation is capable to form hydrogen bonds with the radical-anion, therefore, serves as the basis for creating novel magnetics with a supramolecular structure.

In the contrast to the most RAS TCNQ salts,[7] RAS **1** (CCDC-1850699 in Cambridge Crystallographic Data), see Figure 1c, does not contain stacks made of flat TCNQ particles. In RAS TCNQ there may be no-spin σ-dimers $(TCNQ\text{-}TCNQ)^{2-}$,[1] however RAS **1** is confirmed to contain isolated π-dimers of $(TCNQ)_2^{\bullet-}$ (see Figure 1b). In this dimer, the distance between the middle planes of anion-radicals is 3.24 Å, while the dihedral angle on the symmetry conditions is equal to zero. This contact distance is smaller than the sum of van der Waals radii of carbon atoms, what was confirmed to be typical for planar π-

[a] Dr. T. N. Starodub, Prof. V. A. Starodub
Institute of Chemistry
Jan Kochanowski University
25-405 Kielce, Poland
[b] Dr. E. Čižmár, A. Kliuikov, Prof. A. Feher
Institute of Physics, Faculty of Science
P. J. Šafárik University
Park Angelinum 9, 041 54 Košice, Slovakia
[c] Dr. M. Kozlowska
Institute of Nanotechnology (INT)
Karlsruhe Institute of Technology (KIT)
76344 Eggenstein-Leopoldshafen, Germany
E-mail: mariana.kozlowska@kit.edu

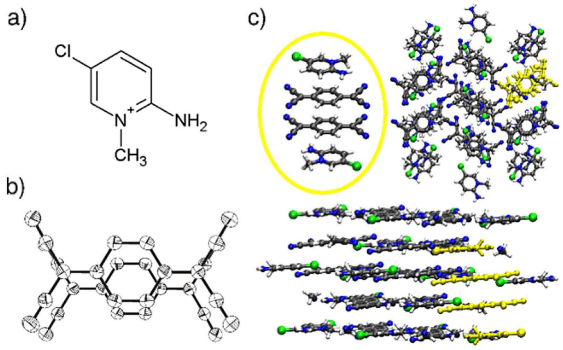

Figure 1. Main components of RAS solvate. Chemical formula of 2-amino-5-chloro-pyridine cation (a). π-Dimers of $TCNQ^{\bullet-}$ anion-radicals in the structure of **1** (b). Visualization of the crystal structure of RAS **1** (c).[6]

conjugated radicals with pancake bonding.[8] We have also noticed that interplanar spacing in the dimer is the same, as in the low temperature phase of RAS of $K^+(TCNQ)^{\bullet-}$, where the reason of dimerization is Peierls instability of TCNQ columns.[9] In our case, the dimers are not parts of long stacked columns,[10] and thus, Peierls dimerization does not occur here.

The formation of isolated $(TCNQ)_2^{\bullet-}$ π-dimers (see Figure 1b,c) was also shown in our previous work on RAS with the $[Mn(phen)_3](TCNQ)_2 \cdot H_2O$ composition.[5a] This salt has AFM behavior, which was explained by dimerization of stacks made of anion-radicals.

Our new RAS **1** contains diamagnetic cations and $(TCNQ)_2^{\bullet-}$ radical-anion π-dimers, therefore, its magnetic properties may be defined only with the latter component. In the present investigation, we use unrestricted density functional theory (DFT) calculations to explain the reason of $(TCNQ)_2^{\bullet-}$ radical-anion π-dimers formation in RAS (N–CH_3–2-NH_2–5Cl–Py)(TCNQ)(CH_3CN) solvate. At the same time, we analyze magnetic susceptibility and magnetization of RAS to show the performance of the material in the antiferromagnetic experiments.

In order to estimate an energy difference between the singlet (ground) and the excited triplet states in RAS pairs of **1**, we have performed quantum-mechanical calculations by means of the density functional theory (DFT). The packing of TCNQ anion π-radicals in TCNQ radical-anion salts was analyzed by Huang et al.,[11] where the intermolecular covalent π-π bonding term in the π-dimers of $(TCNQ)_2^{\bullet-}$, known also as pancake bonding,[8] was estimated and the intermolecular distance between the monomers of approximately 3.3 Å was found as the optimal one. An orbital correlation diagram for π-dimers was also presented (see Scheme 1). It shows the splitting of the orbital levels upon the interactions of two monomers in a dimer.

According to this diagram, bonding in a dimer is formed as a result of overlapping the SOMO orbitals (single occupied molecular orbitals, depicted as single occupied LUMO in Scheme 1). Then, the measure of the excitation energy to the triplet state can be considered as a value of $2|\beta^*|$. Indeed, $2|\beta^*|$ is the dimer level splitting, which reflects the overlap between the two LUMOs of TCNQ.[11] It is the measure of the charge transfer integral, *i.e.* electronic coupling element, responsible for the charge transfer properties of RAS.[12] This integral in the cofacial dimer configuration, as is observed in RAS **1** (depicted in Figure 1b), is the half of the energy

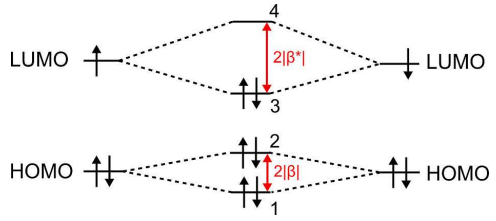

Scheme 1. Orbital correlation diagram from TCNQ anion-radicals to $(TCNQ)_2^{2-}$ showing the dimer level splitting $2|\beta|$ and $2|\beta^*|$ for the HOMO- and LUMO-derived dimer orbitals, respectively. LUMO becomes SOMO when it is singly occupied. Orbital No 3 is the bonding combination of the two SOMO orbitals.[11]

difference between the splitting orbitals.[13] The $2|\beta^*|$ values of the ethylene π-dimers, as also several TCNQ salts, were calculated by Huang and Kertesz.[13] They reported that the values of the dimer level splitting depend on the used quantum-mechanical method and the basis set type. For example, semiempirical calculations by ZINDO/S-method for ethylene π-dimers give a value of $2|\beta^*|$ equal to 0.600 eV, while $2|\beta^*|$ in Hartree-Fock method is 1.631 eV. Becke's three parameter hybrid functional with Lee-Yang-Parr correlation, *i.e.* B3LYP functional, with 6–31G* basis set gives a value of $2|\beta^*|$ of 1.163 eV. It is seen that the uncertainty in the theoretical value of $2|\beta^*|$ is very large, however, DFT results in the proper energy splitting values.[12,13] Therefore, we investigate the formation of dimers from radical anions of TCNQ with unrestricted DFT calculations using B3LYP functional[14] with aug-cc-pVTZ[15,16] basis set and Grimme D3 dispersion correction[17] with Becke-Johnson (BJ) damping.[18] We performed all calculations using Turbomole V.7.1 program package.[19] We consider both, singlet and triplet states of the formed anion pair in the single point calculation of the dimer taken from the crystal structure of RAS **1**.[6] The resulting interaction energy, calculated by the supermolecular approach and corrected for the basis set superposition error (BSSE) using the counterpoise method,[20] is positive: 1.63 eV for singlet and 1.96 eV for triplet states (see Table 1). This indicates not preferable TCNQ cofacial π-dimer formation. It is mainly caused by the Coulomb repulsion between the anion-radicals molecules in the TCNQ π-dimer.

Despite these interactions, which are significantly screened by the cation environment, the dimer is formed due to the strong π-stacking interactions, termed as pancake bonding,[8] as was also reported by Huang et al.[11] using statistical analysis of different TCNQ packing types and by groups of, for example, Kertesz,[8f,g,h] Novoa and Miller.[8b,c,e] This bonding originates from the overlap of the two SOMO orbitals, as depicted in Scheme 1, and its interaction energy is higher than usual vdW interactions, *e.g.* −14–−17 kcal/mol for $(TCNE)_2^{2-}$ dimer, calculated using multireference averaged quadratic coupled-cluster method.[8h] Visualization of the π-π-interactions in the TCNQ dimer is shown in Figure 2a as the noncovalent interaction surface

Table 1. Interaction energy in the singlet and triplet multiplicity state of TCNQ π-dimer with the corresponding dimer level splitting, $2|\beta|$, $2|\beta^*|$, and electronic coupling element, J, between the frontier orbitals of TCNQ in a dimer. Higher energy value characterizes less stable state of the system, while higher electronic coupling reflects higher electron density overlap between the interacting orbitals. Unrestricted DFT calculations were performed using B3LYP with aug-cc-pVTZ basis set and def2-TZVP basis set[21] for comparison. To show an impact of the basis set superposition error (BSSE) on the interaction energy values, both corrected and pristine values of the energy are listed. All values are given in eV.

$(TCNQ)_2^{2-}$	E_{inter}	E_{inter}^{BSSE}	$2\|\beta\|$	$2\|\beta^*\|$	J_{HOMO}	J_{LUMO}
			aug-cc-pVTZ			
singlet	1.595	1.627	0.771	1.370	0.385	0.685
triplet	1.927	1.959	0.665	0.758	0.332	0.379
			def2-TZVP			
singlet	1.620	1.644	0.770	1.370	0.385	0.682
triplet	1.948	1.972	0.665	0.755	0.332	0.377

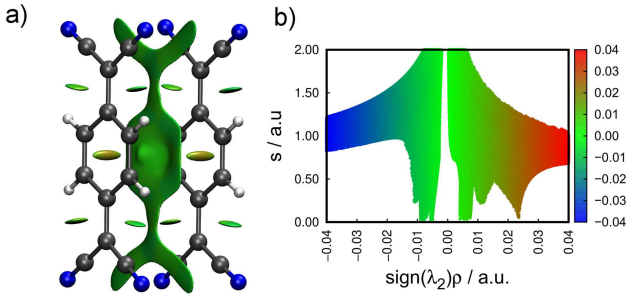

Figure 2. π-π-interactions in $(TCNQ)_2^{\bullet-}$ dimer, truncated from the crystal structure of **1**. Visualization of intermolecular noncovalent interactions (NCI) between neighboring monomers marked with green color (a). The depicted NCI surface corresponds to the reduced density gradient of 0.5 a.u. NCI plot: the relationship between reduced density gradient (s) and the sign of the second eigenvalue (λ_2) of the electron density Hessian, as described in [22, 23] (b). Values of the reduced density gradient approaching 0 a.u. in the electron density range of $-0.01 < \rho < 0.01$ indicate strong inter-radical interactions based on the π−π stacking, *i.e.* pancake bonding.

depicted in green. These interactions, calculated using the noncovalent interaction (NCI) index,[22,23] enable high electron density overlap (reduced density gradient is approaching 0 a.u., see Figure 2b), and therefore, multicenter inter-radical contacts[8] that lead to better electronic coupling (half of the $2|\beta^*|$ value, *i.e.* J_{LUMO} in Table 1) of the SOMO orbitals of TCNQ in its dimer. This significantly increases the dimer stability and its charge transfer properties in the radical-anion salts.

The frontier orbitals of the of $(TCNQ)_2^{\bullet-}$ dimer, marked as molecular orbital No 3 and 4 in Scheme 1, respectively, are shown in Figure 3a, where high electron density delocalization is visible. In the singlet multiplicity state of the dimer in the gas phase, the coupling between the SOMO orbitals, estimated from the energy splitting[24,25] is 0.68 eV (see Table 1). This is significantly higher coupling that known for the TCNQ crystals with different mutual orientation of the TCNQ monomers in the crystal,[26] what suggests efficient electron transport properties of the TCNQ in the material.

It should be mentioned that the electronic coupling of the SOMO orbitals in the triplet state of the dimer is lower, i.e. 0.38 eV. This, together with more repulsive character of the anion-radical TCNQ π-dimer in a triplet state, results the triplet state to be less energetically stable (by 0.33 eV) than the singlet one. The dimer level splitting, $2|\beta^*|$, in a singlet state is

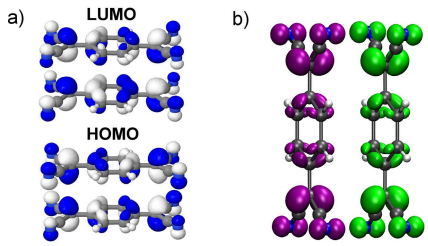

Figure 3. Visualization of the frontier orbitals: HOMO (highest occupied molecular orbital and LUMO (lowest unoccupied molecular orbital), of the TCNQ in a dimer (isovalue of 0.035 a.u.) (a) and spin density localized on the $TCNQ^{\bullet-}$ dimer (b). Alpha orbital (spin up) and beta orbital (spin down) are marked in purple and green and visualized with isovalue of 0.005 a.u.

1.37 eV, confirming more preferable formation of the π-dimers of $(TCNQ)_2^{\bullet-}$ in the singlet state.

The spin density localized on the $(TCNQ)_2^{\bullet-}$ dimer in its singlet multiplicity state is shown in Figure 3b, where the spin-up ($+^1/_2$) and spin down ($-^1/_2$) spin density is marked in purple and green, respectively. Oppositely directed spin densities suggest the AFM behavior of the $(TCNQ)_2^{\bullet-}$ dimer, which is further confirmed by experimental measurements. Such behavior results in the reduction of total magnetic moment observed in magnetic measurements.

Temperature dependence of magnetic susceptibility χT product displays a decrease with decreasing temperature in the whole temperature range (see Figure 4a) with χT of 0.226 cm^3K/mol at 300 K. This is less than expected for one $S = {}^1/_2$ spin of one RAS molecule per formula unit (0.375 $cm^3 \cdot K/mol$ if *g*-factor is fixed to $g = 2$). This behavior indicates the presence of an antiferromagnetic interaction. As shown by theoretical calculations, a strong AFM interaction in the $(TCNQ)_2^{\bullet-}$ π-dimers is induced by the higher stability of the singlet state, by 0.33 eV, in comparison to the triplet state. For such strong AFM interaction, the singlet-triplet excitation energy is high, the dimers are in the singlet state, and the contribution of the magnetic triplet excitation to the total χT is then very small even at the room temperature.

The relatively high value of χT and its gradual decrease towards low temperatures cannot be described by simple Bleaney-Bowers formula for AFM spin dimers. The presence of the relatively high ratio of crystal defects is typical for RAS, resulting in the presence of non-dimerized $(TCNQ)_2^{\bullet-}$ entities,

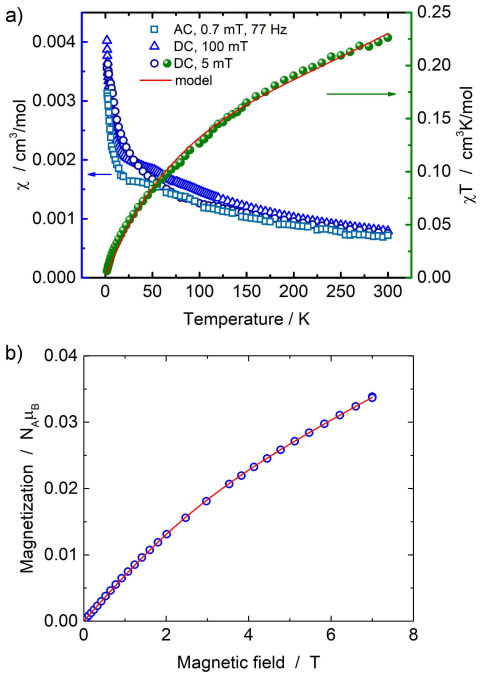

Figure 4. Temperature dependence of magnetic susceptibility (DC mode in fields 5 and 100 mT, AC with 0.7 mT field amplitude) and χT product (DC in field 5 mT), including a fit using the model described in the text (a). Field dependence of magnetization of RAS **1** measured at 2 K (b). The model assumes paramagnetic contribution and weak contribution of correlated spins.

which have been observed in magnetic or electron-paramagnetic resonance (EPR) measurements.[4b,27] As a result, we suggest that χT behavior can be described by the presence of non-dimerized TCNQ.

Although, the Curie-like behavior was observed in the temperature dependence of the susceptibility of RAS **1** (see Figure 4a), the overall temperature dependence of the χT suggests the presence of a sizable AFM interaction due to its gradual decrease towards zero value at 1.8 K. This could be the result of inter-radical interaction between two TCNQ radicals from two neighboring dimers, where the shortest N–N distance between two TCNQ pairs is 3.658 Å. Another contribution could be due to the shift of TCNQ molecules in a dimer, thus effective reduction of the exchange interaction within the dimer and change of the magnetic coupling feature in the molecular crystal.[7] The behavior of the temperature dependence of the susceptibility is also similar to what was previously reported for another RAS with non-stacked TCNQ dimers.[27] Here, two distinct contributions were observed by EPR: *i)* dimerized RAS with a quite high singlet-triplet excitation energy and *ii)* the contribution of non-dimerized spins dominating the low-temperature magnetic properties.

The contribution of non-dimerized molecules often depends on the batch (or even crystal), cooling and heating rate or applied field during the experiment as, for example, is shown in Figure 4a. Since the distribution of the defects is random, it is not possible to use an exact model of the interactions between non-dimerized spins. Therefore, the temperature dependence of the χT was fitted with a model including Bleaney-Bowers formula for AFM dimers (χ_{dimer}) and Curie-Weiss law accounting for an effective AFM interaction between non-dimerized spins (χ_{CW}) in form $\chi_{dimer} = (1\text{-}\rho)\chi_{dimer}/2 + \rho\chi_{CW}$, where ρ is the effective concentration of the non-dimerized spins. The resulting AFM exchange interaction within dimers is J_{dimer} =-1242 K (107 meV), Weiss temperature $\theta = -130.4$ K, and $\rho = 0.2$. This result suggests a relatively strong contribution of non-dimerized spins. The field-dependence of magnetization of **1** measured 2 K, shown in Figure 4b, reaches the value of 0.034 $N_A\mu_B$ only out of 1 $N_A\mu_B$ for fully saturated $S = {}^1/_2$ system. The magnetization can be described by two contributions: paramagnetic contribution, described by Brillouin function representing 1% of well-isolated $S = {}^1/_2$ entities, and linear, which can be tentatively assigned to the weak contribution of AFM dimers or strongly AFM coupled non-dimerized spins.

Theoretical calculations show that the ground state for two TCNQ anion radicals corresponds to non-dimerized particles. In contrast, in the crystal structure with cation, *e.g.* 2-amino-5-chloro-pyridine, the Coulomb repulsions are screened, enabling the formation of the $(TCNQ)_2^{2-}$ π-dimer, stabilized additionally by strong pancake bonding interactions. This corresponds to the obtained experimental data with the π-dimer $(TCNQ)_2^{\bullet-}$ model. Therefore, the formation of these unusual dimers is supported by the crystalline environment and Madelung's energy. DFT calculations confirm the high energy level splitting in a dimer and existence of $(TCNQ)_2^{2-}$ dimer in the basic singlet state, promoting its AFM properties. Strong AFM interactions are also proven by measurements of temperature dependence of magnetic susceptibility and magnetization of the reported RAS. Due to unusual π-dimer formation, antiferromagnetic properties and hydrogen bonding formation in radical-anion (N–CH_3–2-NH_2–5Cl–Py)(TCNQ)(CH_3CN) solvate, the reported RAS is prone to be applied in novel magnetics with a supramolecular structure.

Experimental Section

We have performed the synthesis of RAS using the standard method, based on the reduction of TCNQ by 2-amino-5-chloro-pyridine iodide (*Am*):

$$3/2(N{-}CH_3{-}Am^+I^-) + TCNQ \rightarrow (N{-}CH_3{-}Am)^+ (TCNQ)^{\bullet-} + 1/2(N{-}CH_3{-}Am)^+(I_3)^-$$

Amine *Am* was dissolved in the methyl iodide and the solution was agitated with a magnetic rabble until an amine iodide (N–CH_3–Am^+)I^- had precipitated The yield in terms of the amine was 100%. RAS precipitates were filterd, washed with ether and hexane and dried under vacuum. To grow single crystals and to properly purify the samples recrystallization from acetonitrile was used. Black-violet needle crystals with the length of up to 5 mm were obtained. This gave the title compound in 55% yield. Elemental analysis of the synthesized radical anion salts was performed on a VarioMICRO Superuser analyzer. Calc. C −62.16%, N −24.16%, H −3.48%, Cl −10.19%; found C −62.31%, N −24.21%, H −3.57%, Cl −10.23%. RAS compositions were determined spectrophotometrically, as described in work .[28] It corresponds to the formula (N–CH_3–Am)$^+$(TCNQ)$^{\bullet-}$ (**1**).

The crystallographic data have been deposited to the Cambridge Crystallographic Data Centre (CCDC-1850699). Copies of the data can be obtained free of charge from The Director, CCDC, 12, Union Road, Cambridge CB2 1EZ, UK (fax: +44 1223 336033; e-mail: deposit@ccdc.cam.ac.uk or http://www.ccdc.cam.ac.uk).

Measurements of magnetic susceptibility and magnetization were performed in Quantum Design MPMS3 on nascent polycrystalline samples. The temperature dependence of magnetic susceptibility χ of RAS **1** was determined as the ratio of the measured magnetic moment over the intensity of the applied magnetic field in the temperature range from 1.8 K to 300 K. The sample with mass of 10 mg was packed in a polypropylene capsule held by MPMS3 brass sample holder and measured using so-called vibrating sample magnetometer method to avoid sample holder contribution to the measured magnetic moment. Core diamagnetic susceptibility was estimated using Pascal's constants[29] and subtracted from the total susceptibility.

Acknowledgements

E.Č. and A.F. were supported by VEGA 1/0426/19 and APVV-18-0197. M.K. acknowledges funding by Collaborative Research Center CRC 1176. This work was performed on the computational resource ForHLR II funded by the Ministry of Science, Research and the Arts Baden-Württemberg and DFG ("Deutsche Forschungsgemeinschaft"). We acknowledge support by the KIT-Publication Fund of the Karlsruhe Institute of Technology.

Conflict of Interest

The authors declare no conflict of interest.

Keywords: charge transfer processes · crystal engineering · density functional calculations · magnetic properties · radical ions

[1] a) V. A. Starodub, T. N. Starodub, *Russ. Chem. Rev.* **2014**, *83*, 391–438; b) A. Bosch, B. Bodegom, *Acta Crystallogr. Sect. B* **1977**, *33*, 3013–3021; c) G. J. Ashwell, D. D. Eley, S. C. Wallwork, M. R. Willis, G. F. Peachey, D. B. Wilkos, *Acta Crystallogr. Sect. B* **1977**, *33*, 843–848; d) L. Ballester, A. Gutiérrez, F. M. Perpiñán, M. T. Azcondo, *Coord. Chem. Rev.* **1999**, *190–192*, 447–470; e) K. Mukai, S. Jinno, Y. Shimobe, N. Azuma, M. Taniguchi, Y. Misaki, K. Tanaka, K. Inouec, Y. Hosokoshic, *J. Mater. Chem.* **2003**, *13*, 1614–1621.

[2] T. Mori, H. Inokuchi, *Solid State Commun.* **1986**, *59*, 355–359.

[3] a) Y. Morita, T. Murata, K. Fukui, S. Yamada, K. Sato, D. Shiomi, T. Takui, H. Kitagawa, H. Yamochi, G. Saito, K. Nakasuji, *J. Org. Chem.* **2005**, *70*, 7, 2739–2744; b) B. Mukherjee, M. Mukherjee, *Langmuir*, **2011**, *27*, 17, 11246–11250; c) B. Noda, H. Wada, K. Shibata, T. Yoshino, M. Katsuhara, I. Aoyagi, T. Mori, T. Taguchi, T. Kambayashi, K. Ishikawa, H. Takezoe, *Nanotechnology* **2007**, *18*, 424009 (10pp).

[4] a) D. Šoltésová, G. Vasylets, E. Čižmár, A. V. Fedorchenko, V. Starodub, V. Medviediev, O. Shishkin, O. Bukrynov, A. Feher, *Inorg. Chim. Acta* **2018**, *471*, 272–279; b) D. Šoltésová, E. Cižmár, G. Vasylets, V. A. Starodub, A. Feher, *Acta Phys. Pol. A* **2017**, *131*, 925–927; c) D. Šoltésová, G. Vasylets, E. Čižmár, M. Botko, V. Cheranovskii, V. Starodub, A. Feher, *J. Phys. Chem. Solids* **2016**, *99*, 182–188.

[5] a) G. Vasylets, V. A. Starodub, A. Feher, M. Kajnakova, R. Zboril, J. Tucek, H. Metz, I. Potocnak, *Synth. Met.* **2014**, *194*, 7–10; b) T. N. Starodub, *Russ. J. Appl. Chem.* **2018**, *91*, 473.

[6] T. N. Starodub, D. Fenske, O. Fuhr, O. N. Kazheva, V. A. Starodub, *Crystal. Reports* (under review).

[7] G.-X. Liu, H. Xu, X.-M. Ren, W.-Y. Sun, *CrystEngComm* **2008**, *10*, 1574–1582.

[8] a) S. Suzuki, Y. Morita, K. Fukui, K. Sato, D. Shiomi, T. Takui, K. Nakasuji, *J. Am. Chem. Soc.* **2006**, *128*, 8, 2530–2531; b) I. Garcia-Yoldi, J. S. Miller, J. J. Novoa, *J. Phys. Chem. A* **2009**, *113*, 7124–7132; c) J. J. Novoa, J. S. Miller, *Acc. Chem. Res.* **2007**, *40*, 189–196; d) Y. Jung, M. Head-Gordon, *Phys. Chem. Chem. Phys.* **2004**, *6*, 2008–2011; e) J. J. Novoa, P. Lafuente, R. E. Del Sesto, J. S. Miller, *Angew. Chem. Int. Ed.* **2001**, *40*, 2540–2545; f) Z.-h. Cui, H. Lischka, H. Z. Beneberu, M. Kertesz, *J. Am. Chem. Soc.* **2014** *136*, 37, 12958–12965; g) M. Kertesz, *Chem. Eur. J.* **2019**, *25*, 400–416, h) Z.-h. Cui, H. Lischka, T. Mueller, F. Plasser, M. Kertesz, *ChemPhysChem* **2014**, *15*, 165–176.

[9] M. Konno, T. Ishii, Y. Saito, *Acta Crystallogr. Sect. B* **1977**, *33*, 763–770.

[10] L. B. Coleman, M. J. Cohen, D. J. Sandman, F. G. Yamagishi, A. F. Garito, A. J. Heeger, *Solid State Commun.* **1973**, *12*, 1125–1132.

[11] J. Huang, S. Kingsbury, M. Kertesz, *Phys. Chem. Chem. Phys.* **2008**, *10*, 2625–2635.

[12] B. Baumeier, J. Kirkpatrick, D. Andrienko, *Phys. Chem. Chem. Phys.* **2010**, *12*, 11103–11113.

[13] J. Huang, M. Kertesz, *J. Chem. Phys.* **2005**, *122*, 234707-1–234707-11.

[14] A. D. Becke, *J. Chem. Phys.* **1992**, *96*, 2155–2160.

[15] T. H. Dunning Jr., *J. Chem. Phys.* **1989**, *90*, 1007–1023.

[16] R. A. Kendall, T. H. Dunning, Jr., R. J. Harrison, *J. Chem. Phys.* **1992**, *96*, 6796–6806.

[17] S. Grimme, J. Antony, S. Ehrlich, H. Krieg, *J. Chem. Phys.* **2010**, *132*, 154104-1–154104-19.

[18] S. Grimme, S. Ehrlich, L. Goerick, *J. Comput. Chem.* **2011**, *32*, 1456–1465.

[19] R. Ahlrichs, M. Bär, M. Häser, H. Horn, C. Kölmel, *Chem. Phys. Lett.* **1989**, *162*, 165–169.

[20] S. F. Boys, F. Bernardi, *Mol. Phys.* **1970**, *19*, 553–566.

[21] A. Schäfer, C. Huber, R. Ahlrichs, *J. Chem. Phys.* **1994**, *100*, 5829–5835.

[22] E. R. Johnson, S. Keinan, P. Mori-Sánchez, J. Contreras-García, A. J. Cohen, W. Yang, *J. Am. Chem. Soc.* **2010**, *132*, 6498–6506.

[23] J. Contreras-García, E. R. Johnson, S. Keinan, R. Chaudret, J.-P. Piquemal, D. N. Beratan, W. Yang, *J. Chem. Theory Comput.* **2011**, *7*, 625–632.

[24] J.-L. Brédas, D. Beljonne, V. Coropceanu, J. Cornil, *Chem. Rev.* **2004**, *104*, 4971–5004.

[25] C. Grieco, G. S. Doucette, J. M. Munro, E. R. Kennehan, Y. Lee, A. Rimshaw, M. M. Payne, N. Wonderling, J. E. Anthony, I. Dabo, E. D. Gomez, J. B. Asbury, *Adv. Funct. Mater.* **2017**, *27*, 1703929–1703938.

[26] A. Yu. Sosorev , *Phys. Chem. Chem. Phys.* **2017**, *19*, 25478–25486.

[27] M. C. Grossel, S. C. Weston, *Chem. Mater.* **1996**, *8*, 977–980.

[28] D. V. Ziolkovskiy, A. V. Kravchenko, V. A. Starodub, O. N. Kazheva, A. V. Khotkevich, *Funct. Mater.* **2005**, *12*, 577–582.

[29] J. C. O'Connor, *Magnetochemistry – advances in theory and experimentation*, in: Stephen J. Loppard, Progress in Inorganic Chemistry, NY. **1982**.

Manuscript received: May 21, 2019
Revised manuscript received: June 28, 2019